HiSST: 3rd International Conference on
High-Speed Vehicle Science Technology
14 -19 April 2024, Busan, Korea

Study of liquid-vapor phase change process inside porous cooling device for hypersonic vehicle

Rui MA, Shibin LI[1], Zhongwei WANG, Lin WANG, Qingyang Guo

Abstract

Aiming at the thermal control problem of the key parts in hypersonic vehicle, an adsorption autonomous cooling device based on porous media was designed. The transient behavior of two-phase flow and heat transfer inside porous media was studied numerically and experimentally in this paper. The two-phase mixing model was used in the numerical method and verified by the visualization experiment. The results shows that the heat transfer performance of adsorption autonomous cooling device was more significant under the hot-end exhaust design. It shows that the temperature of cold-end was still within 100 ℃ at 1500 s. Moreover, the motion direction of the vapor phase was always opposite to gravity, and the flow direction of the liquid phase was squeezed by the vapor phase and related to the outlet position. The liquid working fluid was more strongly bound by the pore structure. Furthermore, the liquid working medium was further vaporized near the interface after the formation of the two-phase mixing zone.

Keywords: *Hypersonic vehicle, Adsorption autonomous cooling, Liquid-vapor phase change, Porous struction, Mechanism of temperature control*

Nomenclature

Nomenclature

C_p	specific heat of fluid（J/kg K）
$f(s)$	hindrance function, Table 1
g	gravitational acceleration (m/s2)
h	enthalpy (J/m3)
h_{fg}	latent heat of phase change (J/kg)
H	height of the simulation domain (m)
$J(s)$	capillary pressure function
K	permeability of the porous medium (m2)
p	pressure (Pa)
s	liquid saturation
t	time (s)
T	temperature (℃)
u	velocity vector (m/s)（superficial or Darcian velocity vector）

Greek symbols

γ	Advection correction coeficient (two-phase advection correction coefficient, Table 1)
ρ	density (kg/m3)
ε	porosity
μ	dynamic viscosity (kg/m s)
ν	kinetic viscosity (m2/s)
Ω	effective heat capacitance ratio
Γ_h	diffusion coefficient in enthalpy equation

Subscripts

l	liquid
v	vapor
s	solid
o	initial state
sat	saturated state

[1] Hypersonic Technology Laboratory, *National University of Defense Technology, 410073, (Changsha City, Hunan Province), P.R. China. lishibin104@163.com*

1. Introduction

With the development of vehicle engines, materials and other aspects, the flight time and speed of hypersonic vehicles continue to increase [1]. The 'thermal barrier' problem caused by air compression/stagnation/high-speed friction poses new challenges to the thermal protection design of aircraft. Thermal protection design has become a key factor restricting the success or failure of flight, especially for the key stagnation points such as nose cone, inlet leading edge and rudder leading edge [2].

The active thermal protection takes away most or all of the heat through the convection of the cooling medium, which is mainly divided into convective cooling [3], transpiration cooling [4], film cooling and so on [5]. It demonstrates high cooling efficiency and broad application prospect [6]. However, it needs to carry a large number of cooling refrigerants, liquid storage containers, and external drive devices when facing long-endurance flight conditions, which will greatly increase the weight of the vehicle and the complexity of the system. This further adversely affects the overall design of high-speed vehicles. Numerous previous studies have shown that active cooling techniques accompanied by phase changes are more efficient in thermal control. Furthermore, the fluid heat transfer area is enlarged and the heat transfer effect is enhanced in the thermal protection structure based on porous media. In addition, it is one of the effective ways to improve the cooling efficiency of the coolant through the reasonable design of the substrate flow channel and the selection of the fluid working parameters [7-8]. For example, Wu Yadong et al. conducted an experimental study on the porous media transpiration cooling system using liquid water as a coolant. It was found that the heat control effect was obvious by utilizing the heat absorption property of water phase change process for transpiration cooling [4]. A smooth gradient pore structure was prepared by Zhilong Cheng et al. using additive manufacturing technology. Relevant experimental studies have found that the gradient porosity exhibits better cooling performance than the uniform pore topology. The imbalance of coolant distribution under non-uniform heat flux was improved, consequently, the hot spot temperature was reduced [9]. The bionic self-priming transpiration cooling system was designed by Peixue Jiang et al., which uses structural capillary force to realize self-pumping and self-adaptation of coolant. The research shows that the additional load of the cooling system was reduced. Besides, the system has high cooling efficiency and good stability [10].

Based on this, the flow and heat transfer problems in small-scale spaces such as microchannels and porous structures have attracted the attention and research of a large number of scholars. In terms of experiments, the evaporative cooling performance of a new type of C/SiC porous ceramic with liquid water was studied by Bo Zhang et al., and the evaporative cooling performance was reasonably improved by increasing the material forming pressure [11]. Yinning Zhang et al. [12] used silicon-glass bonding method to fabricate visualization test pieces. The growth and coalescence behavior of bubbles in porous media under heating conditions were studied. The results show that anisotropic porous media has a guiding effect on bubbles, which indicates that it is easier to realize bubble flow pattern control in practical engineering applications. In terms of numerical simulation, there are mainly pore grid model [13-14], VOF [15], multiphase flow model [16], multiphase mixing model (MPMM) [17-18]. Where the multiphase is considered as a binary chemical mixture in the multiphase mixing model. Furthermore, the algebraic relationship for calculating the phase velocity from the mixture velocity field is provided. Therefore, the two-phase characteristics are fully retained in the formula, and it has better versatility and flexibility, and the number of solutions to the control equations is also greatly reduced [17]. The complexity and invisibility of the micro-channel/porosity structure pose certain challenges to experimental observation, model construction, and numerical solution. It is necessary to further carry out mechanism research from various aspects such as visualization experiments methods, pore/macro-scale modeling, and make technical reserves for the design and optimization of high-efficiency heat exchange equipment for high-speed vehicle in the future.

In this paper, aiming at the thermal control problem of high temperature components in the special cabin of advanced vehicle, the mechanism of an adsorption self-cooling device based on porous structure is studied by combining numerical simulation and experiment.

2. Design principle and scheme

Aiming at the problem of thermal control in local high temperature region of long endurance high speed vehicle, a new semi-active cooling temperature control principle was proposed in the preliminary work of our research group. Based on this principle, an adsorption autonomous cooling device was designed, and the feasibility of the scheme was verified by experiments.

As shown in Fig.1, the adsorption self-cooling device consists of a cavity-shaped main structure, porous medium, and some cooling medium. Among them, the porous medium has the characteristics of low density, low thermal resistance and high hydrophilicity, which is used as a carrier to store and bind the liquid cooling medium. Its working principle are as follows: The system realizes the self-pressurization and autonomous cooling cycle by effectively using the thermal energy from aerodynamic heating as the driving force. At the same time, the confinement of the cooling medium is achieved by utilizing the structural characteristics of the porous medium. The spontaneous flow of the two-phase fluid is driven by the phase change, which maximizes the use of the sensible heat and latent heat of the cooling medium, and achieves the purpose of temperature control.

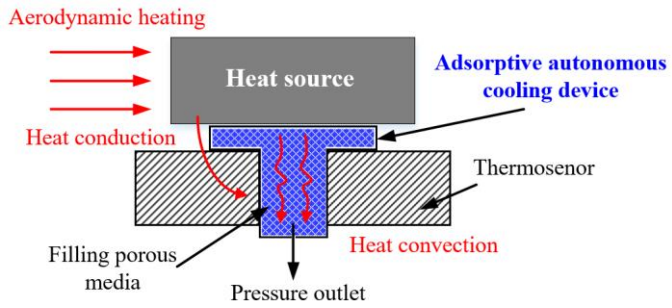

Fig 1. Adsorptive autonomous cooling device and its working principle

The heat transfer performance of the adsorption self-cooling device is affected by many factors, such as material parameters, structural parameters, heat flux density, inclination angle and outlet position. In particular, the effect is manifested as a difference in the flow behavior of the two-phase fluid within porous structure at the macroscopic level. Wherein the outlet position can be set at the hot end or the cold end of the device. The steam further secondary cools the heat source when it is discharged from the hot end. In addition, the steam can be used as the steam source of the jet when it is discharged from the cold end. The two outlet positions have a significant effect on the two-phase fluid flow in the device.

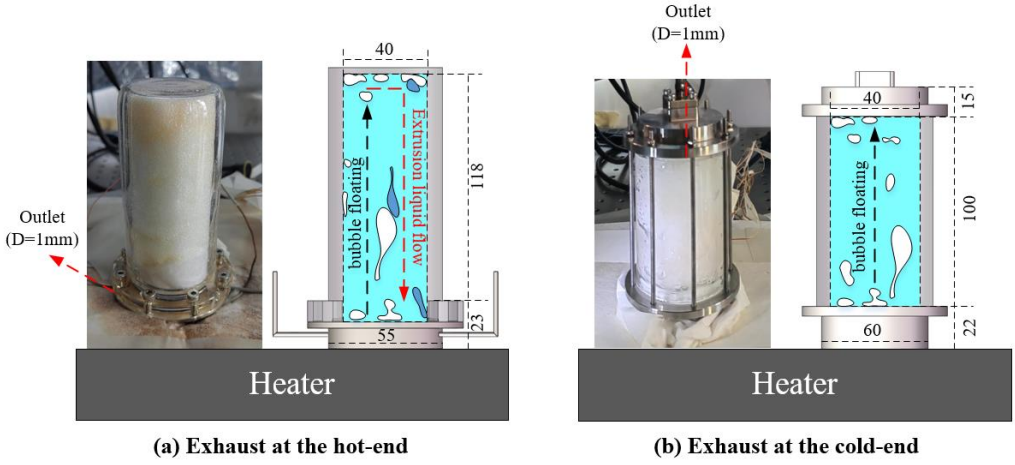

Fig 2. Diagram of outlet position

Based on this, the visual experimental section with different outlet positions are designed, and the heat transfer mechanism of the cooling device is deeply explored. The dimensions and the object of the model are shown in Fig. 2. The high temperature resistant quartz glass is selected to make the visual observation section. In order to ensure sufficient heat absorption, the stainless-steel base is designed as the heat absorption end, which is mechanically sealed with the observation section through sealing

rings and bolts. Polyurethane with a porosity of about 85 % is selected as the porous medium, and liquid water is used as the cooling medium. In addition, the heating surface is coated with quartz cotton felt to reduce the heat loss caused by convection with the outside world. The latent heat of vaporization of saturated water under normal pressure is 2.257×10^3 J/kg, and the basic thermophysical parameters of other related materials are shown in Table 1.

Table 1. Basic physical parameters of materials

Name	ρ [kg/m3]	C_p [J/(kg·K)]	h [kJ/kg]	k [W/(m·K)]			
				25°C	100°C	300°C	500°C
stainless steel	7800	501.6	/	15.3	16.3	18.8	21.8
quartz glass	2200	900	/	1.65			
saturated water	999.7	4220	419	0.68			
saturated steam	0.598	2028	2676	0.0248			
polyurethane	15	150	/	0.02			
quartz cotton felt	100	600	/	0.041			

The porous structure increases the heat transfer area of the cooling medium, and the cooling efficiency of the device is also improved. However, due to the opacity and complexity of the porous matrix, there are considerable difficulties and challenges in fully visual observation. Therefore, the combination of numerical simulation and visualization experiments is adopted, and the flow behavior of two-phase fluid is observed and analyzed in more detail, which is particularly important to reveal the heat transfer characteristics of porous cooling device.

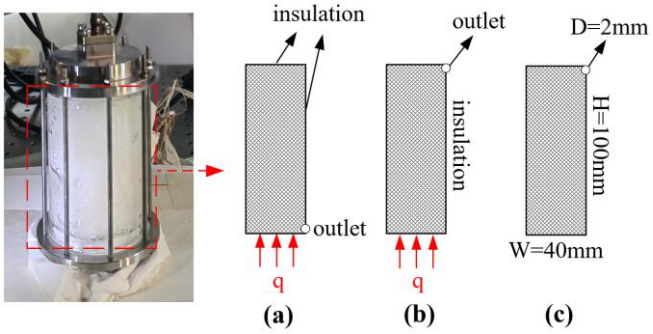

Fig 3. Simplified model: (a) outlet at the cold-end; (b) outlet at the hot-end;(c) related dimension

Due to the large difference in heat transfer performance caused by the metal connecting section, the two-dimensional simplified model of the quartz glass section in the experimental pieces is intercepted for calculation. The model and its size are shown in Fig. 3. In the calculation, the porous medium is assumed to be isotropic and uniform, and the atmospheric pressure is set at the outlet, which is located at the bottom (hot end) and top (cold end) of the right wall respectively. In addition, the heat flux at bottom is 100 Kw/m^2, and other walls are set to adiabatic and impermeable conditions.

3. Numerical method and visualization experimental system

3.1. Numerical method and validation

The fluid channels in the porous structure are small and interconnected. At the same time, the energy equation of two-phase fluid flow and heat transfer is highly nonlinear, which poses a great challenge to meshing, model construction and solution. In this paper, the two-phase mixing model (TPMM) is used to model the two-phase flow and heat transfer process in porous media. In addition, the transient calculation is adopted, and the corresponding mass conservation equation, momentum conservation equation and energy conservation equation are as follows [17,19]:

$$\varepsilon\frac{\partial\rho}{\partial t}+\nabla\cdot(\rho u)=0 \tag{1}$$

$$u=-\frac{K}{\mu}\left[\nabla p-(\rho_k-\rho_o)g\right] \tag{2}$$

$$\Omega\frac{\partial h}{\partial t}+\nabla\cdot(\gamma_h uh)=\nabla\cdot(\Gamma_h\nabla h)+\nabla\cdot\left[f(s)\frac{K\Delta\rho h_{fg}}{\nu_v}g\right] \tag{3}$$

In order to preserve the two-phase characteristics in the liquid phase transition process, the temperature and saturation relationship in the two-phase region are supplemented as follows:

$$T=\begin{cases}\dfrac{H+2\rho_l h_{\mathrm{vsat}}}{\rho_l c_l} & H\leqslant-\rho_l(2h_{\mathrm{vsat}}-h_{\mathrm{lsat}})\\ T_{\mathrm{sat}} & -\rho_l(2h_{\mathrm{vsat}}-h_{\mathrm{lsat}})<H\leqslant-\rho_v h_{\mathrm{vsat}}\\ T_{\mathrm{sat}}+\dfrac{H+\rho_v h_{\mathrm{vsat}}}{\rho_v c_v} & -\rho_v h_{\mathrm{vsat}}<H\end{cases} \tag{3}$$

$$\mathrm{s}=\begin{cases}1 & H\leqslant-\rho_l(2h_{\mathrm{vsat}}-h_{\mathrm{lsat}})\\ -\dfrac{H+\rho_v h_{\mathrm{vsat}}}{\rho_l h_{fg}+(\rho_l-\rho_v)h_{\mathrm{vsat}}} & -\rho_l(2h_{\mathrm{vsat}}-h_{isat})<H\leqslant-\rho_v h_{\mathrm{vsat}}\\ 0 & -\rho_v h_{\mathrm{vsat}}<H\end{cases} \tag{4}$$

The calculation is modeled and calculated by COMSOL Multiphysics 6.0, in which the energy equation is written and set by the partial differential function module. In order to reduce the difficulty of the solution and improve the convergence of the solution, the vapor is assumed to be an ideal gas, and the variables in each iteration process are updated by the automatic highly nonlinear Newton iteration method.

Based on the above control equations and related variable relations, the two-phase flow heat transfer problem in porous media is numerically verified. The numerical simulation method is verified based on the experimental results of two-phase fluid flow and heat transfer in porous materials in Reference [20]. In this experiment, sodium calcium glass beads with a diameter of 0.5 mm were selected as porous materials. The porosity and absolute permeability were 0.42 and $2.9*10^{-10}$ m^2, respectively, and a local heat source was added to the bottom of the porous matrix. Corresponding to the experiment, the size and boundary conditions of the numerical calculation model are shown in Fig.4.Transient calculation is used with a duration of 1000 s.

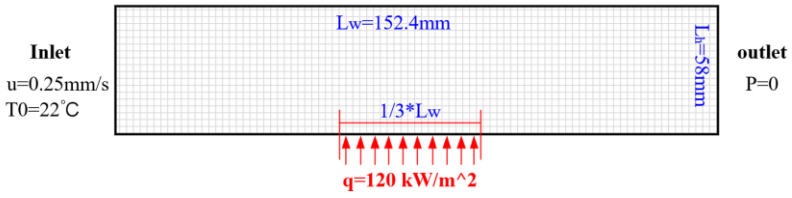

Fig 4. Numerical verification model

The saturation distribution cloud diagram is obtained by simulation, as shown in Fig.5. The results show that the mixed two-phase flow field extending downstream from the heat source can be observed in the experimental and simulation images. Moreover, the steam content in the two-phase mixing zone reaches the maximum near the heat source, and the corresponding saturation is the lowest. The interface between the two-phase mixing zone and the single-phase flow field is bow-shaped, which is because the inlet fluid has a certain flow rate. The leading edge of the bow interface is slightly forward in the numerical simulation, and the saturation near the heat source is also large. It is considered that the steady state has been reached in the test, while the transient calculation is used in the numerical simulation. At the same time, the simulation is based on the assumption of thermal equilibrium, which

leads to a certain difference in the distribution of vapor-liquid phase content. However, the distribution of two-phase fluid is well fitted with the visualization test in general.

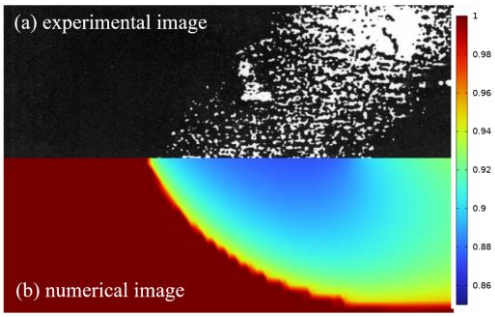

Fig 5. Comparison of experimental and simulation results

3.2. Experimental system and scheme

In this paper, a visual experimental platform is built, and the mechanism of two-phase flow and heat transfer in porous structures is studied. The experimental system is shown in Fig.6, which mainly includes heating system, measurement system and data processing system. Among them, the heating system adopts a constant temperature heating platform (~750 °C); The measurement system mainly includes infrared thermal imager, thermocouple, high-definition camera and pressure scanning valve.

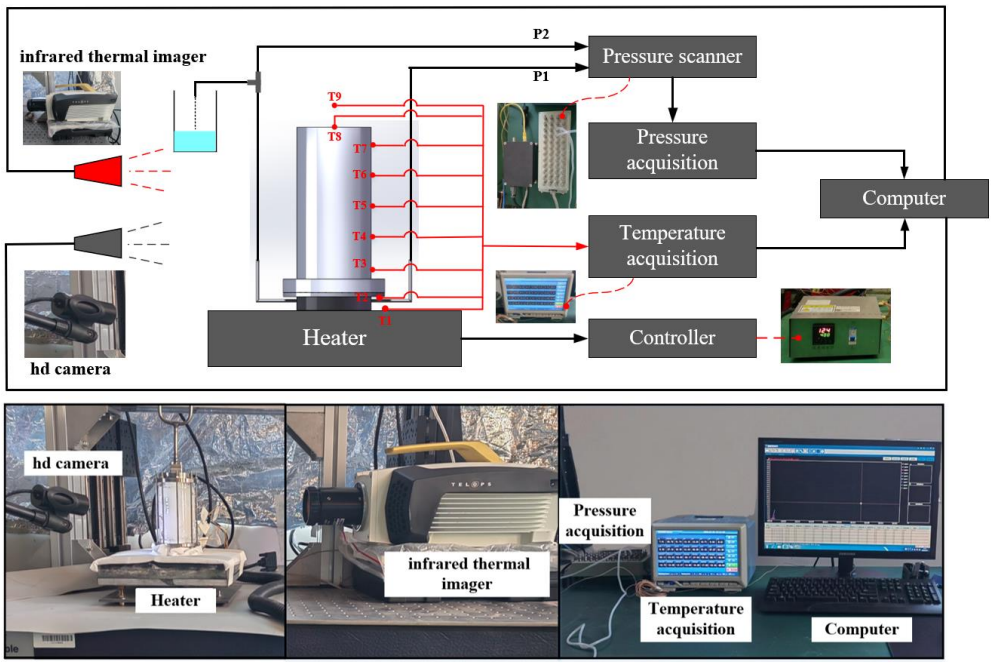

Fig 6. Visualization experimental system

During the experiment, the experimental pieces are heated by the constant temperature heating platform, the temperature field evolution process of the experimental pieces is recorded by infrared thermal imager and thermocouple. At the same time, the flow field evolution process in the experimental pieces is recorded by high-definition camera, and the pressure is collected by pressure scanning valve. Finally, the change process of temperature and pressure is recorded and saved by data acquisition software. Among them, there are nine key measuring points for thermocouple monitoring, which are distributed on the heating platform (T1), the outer wall of the experimental pieces (T2~T8), and the ambient temperature is recorded by the T9.

The method of controlling variables is adopted to explore the influence of the outlet position under the same heating conditions and filling conditions. The specific experimental conditions are shown in Table 2:

Table 2. Experimental condition

Num.	Thermal control scheme	Weight (g)			Position of outlet	Pressure of outlet (MPa)	Heating temperature (°C)
		water	porous medium	total			
Case 1	Adsorption	160	26~30	186~190	Hot-end	0.1	400
Case 2	Adsorption	160	26~30	186~190	Cold-end		

4. Results and discussion

The temperature field and flow field of the cooling device are explored by the combination of experiment and simulation. Then, the two-phase fluid flow and heat transfer law in the porous structure at different outlet positions are analyzed. Further, the heat transfer mechanism of the adsorption self-cooling device is revealed.

4.1. Feature of heat transfer under hot-end exhaust conditions

The temperature field distribution of the cooling device is closely related to the phase change characteristics of the internal cooling medium, and the temperature field change is significantly affected by the exhaust position. As shown in Fig. 7, under the hot end exhaust condition, the temperature of the hot end rises to 45 °C at 400 s, and the temperature of the cold end is equivalent to the ambient temperature. At this time, the heat transfer is mainly by conduction. Then, a small cluster temperature rise area appears in the center of the cold end at 800 s. The temperature in this area is about 40 °C, which is more than 10 °C higher than the surrounding temperature. At this time, the temperature of the hot end reaches 85 °C. This explains the vaporization of the cooling medium near the hot end, where discrete bubbles cluster into larger bubbles and break free from the porous structure to move towards the cold end, resulting in the formation of a clustered temperature rise region. With the accumulation of heat, the vaporization intensifies and the vapor expands to the cold end. The temperature and range of the clustered temperature rise region also expanded rapidly, and the core temperature of the area reached 64 °C at 865 s. At this time, the temperature field distribution in the device is extremely inhomogeneous. This inhomogeneity is related to the vapor-liquid phase distribution. This means that the vapor expansion capacity is strong in the early boiling stage. Bubbles constantly move in the direction opposite to gravity, under the action of density difference. At the same time the liquid is driven by vapor pressure for convective heat transfer, the two phases interact in a narrow porous channel, and the mixture is formed. This temperature inhomogeneity gradually weakened with the accumulation of heat. At 1100 s, the temperature of the hot end and the middle section is close to the same. At this time, a large amount of liquid is still bound in the pore structure, which is carried and squeezed by the vapor flow to the outlet, and gradually evaporates after 1500 s.

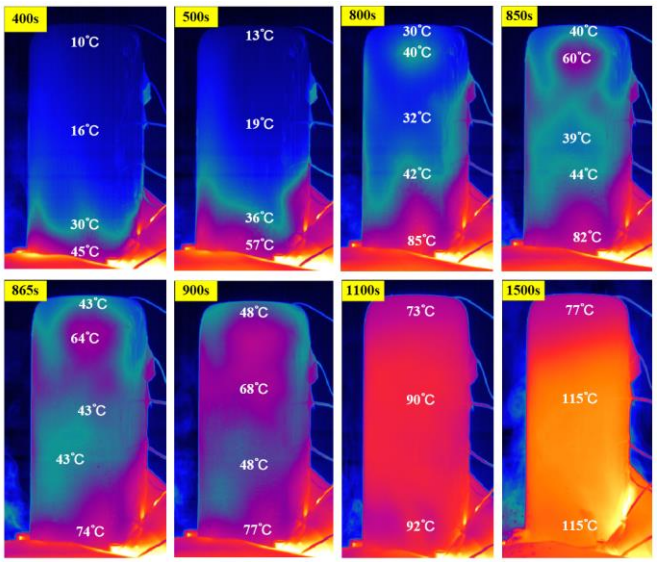

Fig 7. The evolution process of temperature field in Case 1

The phase distribution and flow field evolution process under hot-end exhaust conditions are analyzed and studied more closely by numerical simulation. As shown in Fig. 8, three characteristic points P1~P3 are established on the central axis of the cooling device, which are used to analyze the temperature field and phase field evolution process, and then the heat transfer characteristics are analyzed and summarized. It can be seen that the overall temperature of the device remains below the boiling point at 1400s under this condition. Combined with the saturation curve, it can be seen that the minimum saturation near the hot end is 0.85, and the other measuring points saturation is always 1. This indicates that the vaporization is only carried out near the heat source, the vaporization and flow of the working fluid are slow.

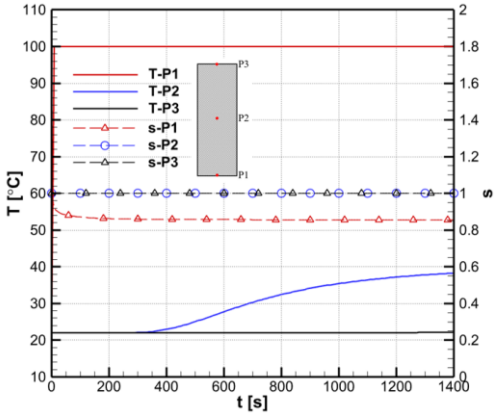

Fig 8. Temperature and saturation change at hot-end discharge

The vapor and liquid phase velocity distribution under the hot end exhaust condition is shown in Fig. 9. It can be seen that the fluid disturbance occurs near the hot end surface. Although the velocity of vapor motion and its involved area are very small at 20 s, the liquid phase is heated by convection and moves to the cold end as a very low speed. The range of vapor migration at the hot end is expanded at 100 s, and its movement direction points to the interface between the two-phase mixing zone and the saturated liquid phase, and the movement speed is distributed from high to low at the hot end to the interface. The velocity direction of the liquid phase is clearly bounded at the interface, which is opposite to the vapor movement direction in the two-phase mixing zone. However, there are three directions outside the two-phase mixing zone: pointing to the cold end, lateral movement, and pointing to the outlet. As the heating continues, the two-phase mixing zone continues to expand and the interface rises. However, the movement trend of the liquid outside the two-phase mixing zone is the same.

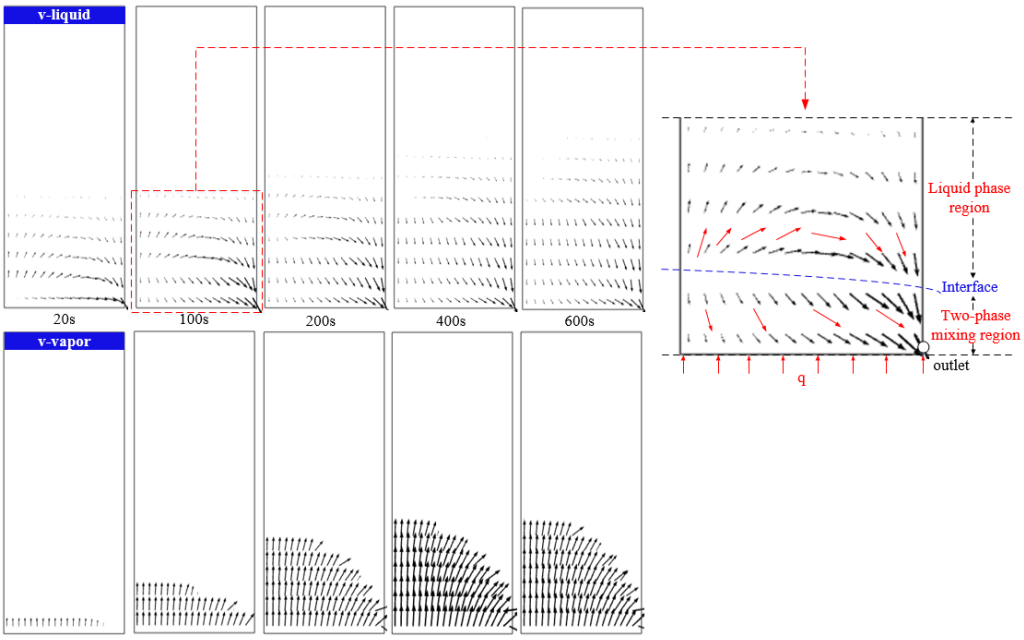

Fig 9. Vapor-liquid phase transport paths during hot-end discharge

This is analyzed in relation to the pressure distribution during the vaporization process. The pressure is lower near the outlet, while the vaporization pressure is higher near the interface between the two phases. As a result, near the interface of the two phases, the saturated liquid will be pushed by the vapor towards the cold end and outlet where the pressure is much lower. Due to the lowest pressure at the outlet and its location near the heat source, the liquid pointing towards the cold end shows a lateral movement and eventually points towards the outlet, while the liquid in the two-phase mixing zone also moves to the outlet due to the influence of the vapor expansion pressure difference. The low liquid motion velocity and the significantly higher vapor velocity throughout the computational domain indicate that the pore structure binds the liquid more, and the vapor flow drives the liquid towards the low-pressure region, then ultimately towards the exit direction.

4.2. Feature of heat transfer under cool-end exhaust conditions

It is different from the hot end exhaust, when the outlet is set at the cold end, the steam flow can be observed to climb along the two sides of the wall toward the cold end at the moment of 300 s. Its heat is transferred downstream faster, and a localized high heat zone appears at the left wall at the moment of 400 s, with the core temperature reaching 93 °C. At this time, the temperature of the upper right working fluid is 19~22 °C. With the accumulation of vapor, the driving force of steam flow increases and expands to the cold end, while the extruded liquid moves downstream. At the moment of 500 s, it can be observed that the highest temperature in the high temperature zone on the left side reaches 110 °C, while the temperature of the fluid near the upper right side is only 42~47 °C. The temperature difference inside the device is large, and the cold and hot fluids undergo a complex interaction flow while moving together in the direction of the outlet. Then, the temperature in the device tends to be uniform at the moment of 700 s, and the middle section and the hot end are around 113 °C. This indicates that the liquid in the middle and lower part has been completely vaporized and the steam is in a superheated state.

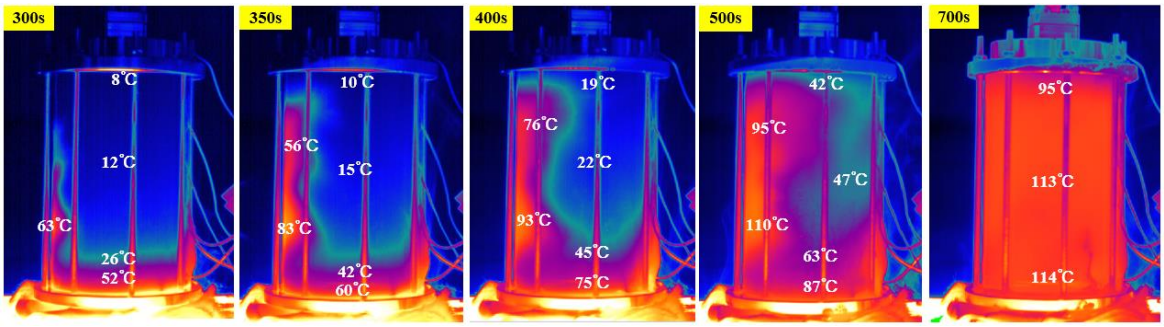

Fig 10. The evolution process of temperature field in Case 2

The numerical simulation of the simplified model under the cold end exhaust condition is carried out, and the variation curves of the temperature and saturation of the feature points with time are shown in Fig.11. It can be observed that the temperature field change in the phase change cooling device is closely related to the saturation degree. The temperature of each point rises rapidly at first, and then remains stable at the boiling point. The saturation curve of each point decreases step by step. Among them, the inflection point of temperature change is close to the first inflection point of saturation curve. Combining the two curves, it is observed that the temperature of the device reaches the boiling point temperature from the hot end to the cold end, and accordingly the saturation degree of each characteristic point decreases in turn. It is considered that the phase change of the cooling medium occurs in each interval, and the working medium enters a more stable mixed state. The stable period of the hot end measuring point is 800 s, and the saturation decreases from 0.85 to about 0.2 after 1125 s. Meanwhile the phase change of the middle measuring point began after 250 s, and the saturation decreased rapidly after 900 s. This indicates that the percentage of vapor at this time increases significantly, and the vapor is able to polymerize into larger bubbles or streams, break through the pore constraints, and quickly reach the exit position. In addition, the cold-end measurement point starts the phase transition at the moment of 664 s, and the rate of saturation decreases from fast to slow, and the cold-end saturation reaches a minimum of 0.07 at the moment of 1400 s, which is close to the vaporized state. This indicates that most of the vapors in the device have been dispersed to the

external environment at this time, and only a very small amount of the working medium is still absorbing heat and vaporizing at the hot end.

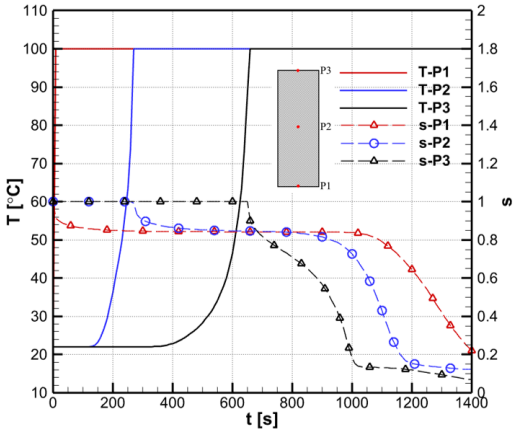

Fig 11. Temperature and saturation change at cold-end discharge

Under the condition of cold end exhaust, the velocity distribution of vapor and liquid is shown in Fig.12. It can be seen that the vapor moves to the cold end, and the direction points to the two-phase interface. The liquid working fluid also moves to the cold end, but with the vaporization of the working fluid, the movement direction of the liquid phase appears a clear boundary at the interface between the mixing zone and the liquid phase zone. It can be seen that the velocity of the liquid phase in the two-phase mixing zone is directed towards the hot end and is very slow. Its flow in the liquid-phase zone is directed towards the cold end and towards the exit position. It can be observed that the two-phase mixing zone expands to the vicinity of the outlet at 600 s, with slow liquid-phase transport and significant lateral motion at the interface. This is due to the lower pressure at the outlet, a part of the liquid originally pointing to the hot end eventually flows to the outlet under the action of pressure difference.

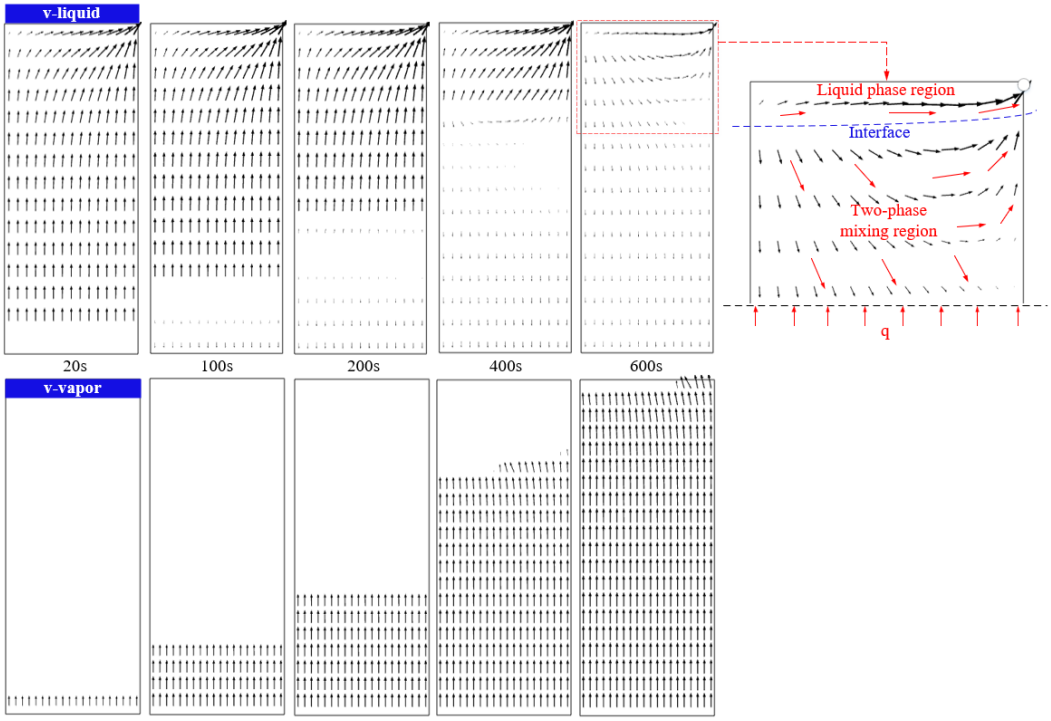

Fig 12. Vapor-liquid phase transport paths during cold-end discharge

This is similar to the experimentally observed phenomenon, where the vapor phase is affected by the density difference to move in the direction opposite to gravity and the liquid phase is further vaporized at the interface of the two phases in both working conditions. As heating continues, the vapor begins to accumulate at the cold end and squeezes the liquid back toward the hot end. But the direction of

liquid movement outside the two-phase mixing zone is directed toward the outlet. The difference is that the liquid phase in the hot-end exhaust condition moves at a significantly lower rate than the cold-end exhaust condition and the coverage area is significantly larger than that under the cold end exhaust condition.

The analysis shows that under the cold end exhaust condition, the outlet is located downstream of the moving direction of the vapor, and the resistance that the vapor needs to overcome is small. At the same time, a large amount of liquid is affected by the pressure difference, and is discharged together with the steam flow after mixing. Therefore, the evaporation time of the cooling medium becomes shorter and the cooling efficiency is lower. However, under the hot end exhaust condition, the outlet is located upstream of the moving direction of the vapor. The vapor is affected by the density difference, and it needs to overcome greater resistance when running in the anti-gravity direction. That is, the flow of two-phase fluid not only needs to overcome the constraints of pore structure, but also needs to overcome the influence of internal pressure and gravity, so the interaction between vapor and liquid is more complex. This also further indicates that the phase change of the working fluid is slower under the hot end exhaust condition, the liquid phase coverage area is larger, and it is not easy to be evaporated at hot end, thus the thermal control performance of the corresponding phase change cooling device is also better.

5. Conclusions

The main conclusions drawn from the simulation calculations and experimental studies of the adsorption autonomous cooling device are as follows:

(1) For the flow of two-phase fluid in porous media, the velocity direction of the vapor phase is always opposite to gravity, and the flow direction of the liquid phase is squeezed by the vapor phase and related to the outlet position. Although it moves to the hot end at a very small speed in the two-phase mixing zone, the overall movement trend points to the outlet;

(2) The pore structure is more capable of binding the liquid, so the transport rate is significantly lower than that of the vapor, and the liquid coverage area under the hot-end exhaust condition is significantly larger than that under the cold-end exhaust condition.

(3) The thermal control performance of the adsorption autonomous cooling device under the hot-end exhaust condition is better. This is because the two-phase fluid flow needs to overcome more resistance and the path is more complicated.

References

1. ZHANG C, WANG Y, YE L: Summary of the Technological Development of Overseas Hypersonics in the Past Ten Years. Tactical Missile Technology. 6, 81-86 (2020)
2. Ai B C, Chen SY, Chen Z, et al: Cognition and discussion on new thermal barrier of hypersonic vehicles. Physics of Gases. 8(4), 1-17 (2023)
3. Xie G , Wang C , Ji T , et al: Investigation on thermal and thermomechanical performances of actively cooled corrugated sandwich structures. Applied Thermal Engineering. 103, 660-669 (2016)
4. WU Y D, ZHU G S, GAO B, et al: An Experimental Study on the Phase-Changed Transpiration Cooling for Active Thermal Protection. Journal of Astronautics. 38(2), 212-218 (2017)
5. XIAN S H, SHANG S F, SHEN Z C, et al: Research progress and development direction of hypersonic film cooling technology. Aerospace Materials Technology. 50(3), 1-10 (2020)
6. Zhu Y, Peng W, Ruina X U, et al: Review on active thermal protection and its heat transfer for airbreathing hypersonic vehicle. Chin J Aeronaut. (2018) https://doi.org/10.1016/j.cja.2018.06.011
7. XU Ruina, LI Xiaoyang, LIAO Zhiyuan, et al: Research progress in transpiration cooling with phase change. J Tsinghua Univ (Sci & Technol). 61(12), 1341-1352 (2021)

8. Silong Zhang, Xin Li, Jingying Zuo, et al: Research progress on active thermal protection for hypersonic vehicles. Progress in Aerospace Sciences. 119, 100646 (2020)
9. Zhilong Cheng, Ruina Xu, Peixue Jiang: Transpiration cooling with phase change by functionally graded porous media. International Journal of Heat and Mass Transfer. 205, 123862 (2023)
10. Peixue Jiang, et al: Experimental investigation of biomimetic self-pumping and self-adaptive transpiration cooling. Biospiration & Biomimetics. 12, 056002 (2017)
11. Bo Zhang, Han Wang, Xiaochao Jin, et al: Novel C/SiC porous ceramic with controllable properties served as transpiration cooling material. Ceramics International. 48(15), 21657-21662 (2022)
12. ZHANG Yinning, WANG Jinqing, FENG Zhi, et al: Growth and coalescience behavior of bubbles in porous media under heating condition. CIESC Journal. 74(4), 1509-1518 (2023)
13. Wang L, Khan A, Erkan N, et al: Critical Heat Flux Enhancement on a Downward Face Using Porous Honeycomb Plate in Saturated Flow Boiling. International Journal of Heat and Mass Transfer. 109, 454–461 (2017)
14. Le K H, Kharaghani A, Kirsch C, et al: Pore Network Simulations of Heat and Mass Transfer inside an Unsaturated Capillary Porous Wick in the Dry-out Regime. Transport in Porous Media. 114(3), 623–648 (2016)
15. Georgoulas A N: Numerical simulation of flow boiling in micro-channels: bubble growth, detachment and coalescence. UK Heat Transfer Conference. (2015)
16. Quintard M, Bletzacker L, Chenu D, et al: Nonlinear, Multicomponent, Mass Transport in Porous Media. Chemical Engineering Science. 61(8), 2643–2669 (2006)
17. Wang C Y: A Fixed-Grid Numerical Algorithm for Two-Phase Flow and Heat Transfer in Porous Media. Numerical Heat Transfer, Part B: Fundamentals: An International Journal of Computation and Methodology. 32(1), 85–105 (1997)
18. Alomar O R: Transient behavior of heat transfer with complete evaporation process in Porous Channel with localised heating using non-Darcian flow and LTNE mode. Heat and Transfer. 11, (2021) https://doi.org/10.1007/s00231-021-03080-3
19. H Y Li, et al: Transient two-phase flow and heat transfer with localized heating in porous media. International journal of Thermal Sciences. 49(7), 1115-1127 (2010)
20. O. T. Easterday, C. Y. Wang: A numerical and experimental study of two-phase flow and heat transfer in a porous formation with localized heating from below. IMECE Proceedings of the ASME Heat Transfer and Fluids Engineering Divisions. 321, 723-732 (1995)